Modeling of light-induced degradation due to Cu precipitation in p-type silicon. I. General theory of precipitation under carrier injection

H. Vahlman,[1,a)] A. Haarahiltunen,[1] W. Kwapil,[2] J. Schön,[2] A. Inglese,[1] and H. Savin[1]
[1]*Department of Electronics and Nanoengineering, Aalto University, Tietotie 3, 02150 Espoo, Finland*
[2]*Fraunhofer Institute for Solar Energy Systems ISE, Heidenhofstr. 2, 79110 Freiburg, Germany*

(Received 30 January 2017; accepted 1 May 2017; published online 15 May 2017)

Copper contamination causes minority carrier lifetime degradation in p-type silicon bulk under illumination, leading to considerable efficiency losses in affected solar cells. Although the existence of this phenomenon has been known for almost two decades, ambiguity prevails about the underlying defect mechanism. In Paper I of this two-part contribution, we propose the first comprehensive mathematical model for Cu-related light-induced degradation in p-type silicon (Cu-LID). The model is based on the precipitation of interstitial Cu ions, which is assumed to be kinetically limited by electrostatic repulsion from the growing Cu precipitates. Hence, growth and dissolution rates of individual Cu precipitates are derived from the drift-diffusion equation of interstitial Cu and used in a kinetic precipitation model that is based on chemical rate equations. The kinetic model is interlinked to a Schottky junction model of metallic precipitates in silicon, enabling accurate calculation of the injection-dependent electric field enclosing the precipitates, as well as the precipitate-limited minority carrier lifetime. It is found that a transition from darkness to illuminated conditions can cause an increase in the kinetics of precipitation by five orders of magnitude. Since our approach enables a direct connection between the time evolution of precipitate size–density distribution and minority carrier lifetime degradation under illumination, a procedure for calculating the Cu-LID-related lifetime as a function of illumination time is included at the end of this article. The model verification with experiments is carried out in Paper II of this contribution along with a discussion of the kinetic and energetic aspects of Cu-LID. *Published by AIP Publishing.*
[http://dx.doi.org/10.1063/1.4983454]

I. INTRODUCTION

Copper is a major contaminant in silicon device technology that has adverse effects for example on state-of-the-art silicon solar cells.[1] Cu can be a problem especially in cast Si due to contamination from the casting crucible.[2] Moreover, fast diffusivity of Cu[3] means easy incorporation into the Si wafer bulk during high-temperature treatments if surface contamination has occurred during previous steps such as wafer sawing[4] or wet processing.[5] In addition, recent efforts to improve the conductivity and reduce the cost of solar cell contacts and interconnects require replacing screen-printed silver with alternative Cu containing alloys, which may increase the risk of cross-contamination on the manufacture line, and, without an efficient diffusion-barrier layer, lead to Cu contamination of the bulk.[6–10]

Unlike many other transition metal impurities (e.g., Fe and Cr), Cu is more harmful in the Si lattice when precipitated than as an interstitially dissolved point defect. The effect of Cu contamination on bulk minority carrier lifetime has been found to depend on the type of doping. In n-type Si, precipitation of Cu occurs even at low contamination levels, which kills the lifetime immediately after in-diffusion and quenching.[11,12] In p-type Si, provided that the Cu contamination level is below the doping level, excess carrier injection (through, e.g., illumination) is necessary to activate lifetime degradation.[11,13–20] For these reasons, Cu-related light-induced degradation (Cu-LID) is only observed in p-type Si. Owing to the fundamental difference in defect activation between n- and p-type Si, especially early contributions[11,13] attributed Cu-LID in p-type Si to a different defect than precipitates, and ambiguity has existed ever since.[21]

P-type silicon, which is the current workhorse of the photovoltaic (PV) industry, can be associated with several different LID mechanisms. Cu-LID has been observed to be a major cause of degradation not only in wafers from the top third of multi-crystalline (mc) Si ingots[22] but also in the corresponding complete solar cells.[23] On the other hand, the well-known light-induced defect composed of boron and oxygen may considerably limit the minority carrier lifetime and consequently the solar cell efficiency if monocrystalline wafers grown with the Czochralski (Cz) process are used.[24–26] Although both impurity Cu and the boron-oxygen (BO) defect can pose a problem in all solar cell architectures, these issues are likely to increase in the future as the industry is currently moving toward passivated emitter and rear cell (PERC) structures whose full utilization requires maximal mitigation of defects limiting the bulk minority carrier lifetime.[27] Transition to the PERC structure has also brought forward a new light-induced defect in mc-Si, whose origin is currently under debate.[28–38] Identification and understanding of the above sources of LID and their underlying defect mechanisms is fundamental when considering methods for their mitigation in solar cells.

[a)]Electronic mail: henri.vahlman@aalto.fi

In this contribution, we focus on Cu-LID, in an attempt to reproduce Cu-LID-related experimental observations through modeling and to provide insights into the corresponding defect mechanism. This article is divided into two papers to enable a sufficiently thorough treatment of theoretical aspects of the proposed model in this Paper I, and to allow a comprehensive discussion of the underlying physical mechanisms behind experimental observations in Paper II.

There are strong reasons, described in Sec. II, to believe that the lifetime-degrading mechanism in p-type Si is a precipitation phenomenon involving charged metallic precipitates. Thereby, a full theoretical model for simulating Cu-LID as a precipitation process is introduced in Sec. III. The model is based on the classical nucleation theory,[39] with precipitates growing or dissolving one atom at a time. Growth and dissolution rates of a diffusion-limited model for spherical precipitates[40] are modified to obey drift-diffusion equations, in order to consider the electric field arising from the precipitate charge. The electric field is determined with a Schottky junction model for metallic precipitates in semiconductors[41–44] (mathematical description is included in the supplementary material), which also allows for the determination of the precipitate-limited injection-dependent minority carrier lifetime. The coupling of the precipitation model with the Schottky junction model is described in detail in Sec. IV. Since time evolution and injection dependence of the BO defect-limited minority carrier lifetime are currently well known,[26,45,46] combining this information with the present model enables the reproduction of full LID curves, that is, minority carrier lifetime as a function of illumination time when both Cu-LID and BO-LID are present simultaneously as separate defects.[21] The validity of the model is investigated in Paper II[76] of this article, using as examples different earlier published and newly observed unpublished aspects of Cu-LID, including dependence on Cu concentration, temperature, intensity, and doping concentration.

II. BACKGROUND FOR THE MODEL

Cu diffuses in Si as a positive interstitial Cu_i^+ ion[47] that pairs easily with dopant B atoms, such that typically a considerable fraction of total interstitial Cu concentration is temporarily trapped in Cu–B pairs.[48] Interstitial Cu has been associated with a shallow donor state at $E_C - 0.15$ eV,[49] and with a very low recombination activity in both n- and p-type Si.[49,50] A considerable amount of Cu (up to the doping concentration) can remain in the interstitial state in p-type Si after quenching from high temperature as was shown through transient ion drift (TID) measurements.[51] On the contrary, immediate precipitation after quenching is observed in n-type Si even with low Cu concentrations.[11] Out-diffusion to wafer surfaces provides a competing sink for bulk precipitation of interstitial Cu. However, this pathway is generally prevented by the presence of a surface oxide, and, due to the positive charge of Cu_i^+, is further inhibited by either a positive native charge or an applied corona charge on the surface.[16,52,53]

Deep level transient spectroscopy (DLTS) studies have shown that Cu precipitates are positively charged in p-type Si and that they introduce a wide band of deep energy levels in the Si band gap, making them highly efficient minority carrier lifetime killers.[54] On the other hand, Cu precipitates are electrically neutral or even negatively charged in n-type Si when the Fermi level is $E_C - 0.2$ eV or above. Thereby, easier Cu precipitation in n- than in p-type Si was explained based on the difference in the Cu precipitate charge state, Cu_i^+ ions experiencing a more pronounced electrostatic repulsion in p-type Si.[54] To support this, Flink *et al.*[55] observed that Cu precipitation is kinetically favored over out-diffusion to the wafer surface when the interstitial Cu concentration is raised high enough to lift the Fermi level above the said neutral level ($E_C - 0.2$ eV). At this level, electrostatic repulsion between Cu_i^+ and the precipitates was considered to be reduced, promoting precipitation over out-diffusion. A similar conclusion was drawn by Sachdeva *et al.*[12] who linked Cu precipitation above the neutral level directly to deterioration of the minority carrier diffusion length.

Based on DLTS results, early Cu-LID observations were associated with a theory involving the dissociation of a Cu complex constituted of substitutional Cu (Cu_s) and interstitial Cu (later this complex was found to consist of four Cu atoms in total[56]) and subsequent formation of recombination-active Cu_s.[11,13] On the other hand, an alternative theory was later suggested where it was deemed plausible that Cu-LID is an electrostatically moderated precipitation process.[15–17] Instead of altering the Fermi-level with the interstitial Cu donor, the charge state of Cu precipitates was speculated to change by a light-induced shift in the quasi-Fermi level of electrons, consequently promoting precipitation. Indeed, the degradation rate of Cu-LID was shown to depend greatly on whether the electron quasi-Fermi level resides above or below the Cu precipitate electroneutrality level of $E_C - 0.2$ eV.[16] Later, involvement of interstitial Cu in Cu-LID was confirmed through a reduction in the related TID signal under illumination that was not explainable by out-diffusion, and it was shown that a charge state change of interstitial Cu under illumination does not control the defect reaction.[18] In addition, activation energy of Cu-LID defect formation has been shown to depend on the doping level,[53] which, considering the dependence of interstitial Cu diffusivity on the B concentration through Cu–B pairing,[48] most likely indicates that the defect formation is diffusion-limited, thus pinpointing at localized extended defects such as precipitates instead of a point defect. Furthermore, a recent temperature- and injection-dependent lifetime spectroscopy study points toward precipitates as the origin of Cu-LID.[57]

Although surface passivation degradation has been suggested as a second Cu-related degradation pathway,[58] it was later shown that Cu-LID is caused by a light-induced increase in bulk recombination.[53] More precisely, no change in surface passivation quality after Cu-LID was observed in the case of thermally oxidized (SiO_2) wafer surfaces.[53] In this contribution, we neglect any surface effects that may hypothetically be present in the absence of a surface dielectric layer or other dielectrics than SiO_2 and focus on the bulk effects of Cu-LID.

On grounds of the above, the most probable hypothesis for the Cu-LID defect formation is a bulk precipitation process limited by electrostatic repulsion between Cu_i^+ ions and Cu precipitates. In essence, the phenomenon resembles that reported by Flink *et al.*[55] and modeled as a precipitation process by Guo and Dunham,[59] where the variation of interstitial Cu concentration was shown to have a great impact on the precipitation rate. In this contribution, we additionally consider light-induced effects by taking into account the effect of varying excess carrier concentration on the precipitate charge state and extend the modeling to the minority carrier lifetime level.

III. THEORY

A. Driving force and mode of precipitation

Precipitation occurs under supersaturation, that is, when dissolved concentration exceeds solid solubility. Dissolved concentration is here the total density of interstitial Cu, including Cu_i^+ and Cu–B pairs. The concentrations of other Cu states and Cu pairs are very low at the relevant temperatures below 200 °C considered in this work (<0.1% of the equilibrium solubility)[60] and are therefore neglected. Gibbs free energy change of forming a precipitate with n atoms can be expressed as[61]

$$\Delta G_n = -nk_B T \ln\left(\frac{C_{Cu_i}}{S_{Cu}}\right) + \Delta G_n^{ex}, \quad (1)$$

where k_B is the Boltzmann constant, T is the temperature, C_{Cu_i} is the total interstitial Cu concentration (including Cu–B), S_{Cu} is the solid solubility associated with large (semi-infinite) precipitates, and ΔG_n^{ex} is the excess Gibbs energy change. The last term in Eq. (1) takes into account forces opposing the precipitate formation, which become notable factors in the energetics in the case of finite-sized precipitates

$$\Delta G_n^{ex} = V_n \Delta G_S + A_n \gamma, \quad (2)$$

where V_n is the volume of the precipitate, ΔG_S is the free energy change per precipitate volume due to strain, A_n is the interface area between the precipitate and silicon matrix, and γ is the corresponding interfacial energy.[62]

Cu precipitation is accompanied by a large volume change. The dominant equilibrium copper silicide phase in Si (η''–Cu_3Si) has a molecular volume 2.3 times larger than that of a Si atom (note that one molecular volume of η''–Cu_3Si includes one Si atom).[3,48] Consequently, homogeneous precipitation is most likely associated with plate-shaped precipitates minimizing the strain energy[63] that can be very high considering that Cu-LID takes place at room temperature (RT). Plate-shaped Cu precipitates associated with homogeneous nucleation have been observed with transmission electron microscopy after fast quenching from high temperatures to RT (i.e., high supersaturation).[54,64,65] On the other hand, formation of spherical Cu precipitates has been reported on heterogeneous precipitation sites such as grain boundaries, dislocations (which can be induced by, e.g., oxygen precipitation), and stacking faults.[64,65]

The Cu-LID defect has not been directly observed by microscopic methods, and therefore, the defect shape and type of nucleation (i.e., homogeneous vs. heterogeneous) remain inconclusive. In Cz samples with intentionally grown oxygen precipitates, Cu-LID has been shown to exhibit degradation behavior that can be interpreted to be characteristic of heterogeneous nucleation.[19] This means that the degradation rate of Cu-LID increased and final lifetime decreased considerably when the density of nucleation sites provided by the oxide precipitates was increased. On the other hand, Cu-LID derived from homogeneous precipitation was speculated to occur in wafers that did not undergo the intentional nucleation site creation stage.[19] Therefore, both the nucleation mode and the defect shape may depend on the studied Si material type and its thermal history. For simplicity, the precipitates were modeled in this work as spheres. As will be shown in Paper II[76] of this article, satisfactory agreement with experiments is obtained with this assumption, showing that at least the effective behavior can be reproduced with the spherical shape.

Many solar grade materials, including mc-Si, are rich in extended defects and impurities that may act as heterogeneous nucleation sites, which means that heterogeneous precipitation is relevant from the PV application point of view. However, modeling of Cu-LID in mc-Si is complicated by extended defects and grain boundaries that often have uneven lateral distribution, which may for example lead to interstitial Cu accumulation in grain boundaries after Cu in-diffusion, or laterally varying nucleation and precipitation behavior. For simplicity, Cu-LID is modeled in this work as a homogeneous precipitation process, and a monocrystalline Si material is used in Paper II[76] for model verification. Here, we note that although homogeneous precipitation is assumed in this work, it does not render the model unusable in the case of materials in which Cu precipitates heterogeneously (e.g., when the density of O precipitates is high), since this can be accounted for material-specifically by lowering the excess energy-related terms ΔG_S and γ in Eq. (2). This, in effect, corresponds to a reduction of the nucleation barrier height and results in an increase in nucleation rate such as expected in the case when density of preferable low-energy nucleation sites is high. Consequently, ΔG_S and γ are considered as effective quantities that are adjusted in Paper II[76] to values providing the best overall correspondence between the model and experimental data obtained using a variety of different Si materials and illumination conditions (the primary aim is to find common values of ΔG_S and γ for all tested materials). Consequences of variation of the nucleation barrier height on degradation kinetics and final degraded lifetime of Cu-LID are discussed further in Paper II[76] of this article.

B. Electrostatic model for charged precipitates

Electrostatics of Cu precipitates is important from two standpoints. First, as described above, electrical interactions between Cu_i^+ and the precipitates are expected to alter

precipitation kinetics. Second, precipitate-limited minority carrier lifetime, τ_{prec}, is determined by interactions between the charged precipitates and charge carriers.

The effect of illumination on precipitate charging is illustrated in Fig. 1, where (a) shows a spherical metallic precipitate composed of n Cu atoms with radius r_n in the η''–Cu_3Si phase embedded in a p-type Si lattice. A Schottky junction with a barrier height $e\Phi_{Bp}$ (where e is the elementary charge) is formed at the interface between the metallic Cu_3Si precipitate and the Si lattice. In thermal equilibrium [Fig. 1(b)], the precipitate is charged with majority carriers so that the Fermi levels of the precipitate and surrounding Si align ($E_F^M = E_F$). This results in an electric field extending from r_n to r_{elec} on the Si side. The corresponding built-in voltage, Ψ_n^S, associated with downward bending of the valence and conduction bands, forms an electrostatic barrier for positively charged Cu_i^+, thus decreasing its concentration at the precipitate surface. This leads to a proportional decrease in the total interstitial Cu concentration, C_{Cu_i}, at the interface since the concentration of Cu–B pairs is directly proportional to $[Cu_i^+]$.[66] Hence, the electrostatic barrier inhibits the growth of the precipitates in the dark at RT. Under illumination (charge carrier injection), the concept of Fermi-level breaks down as external generation causes the separation of E_F into two quasi-Fermi levels, E_{Fn} and E_{Fp}, as illustrated in Fig. 1(c) with a band diagram. As will be shown below, this leads to a reduction in Ψ_n^S, which increases the interface concentration of interstitial Cu and consequently the precipitate growth rate.

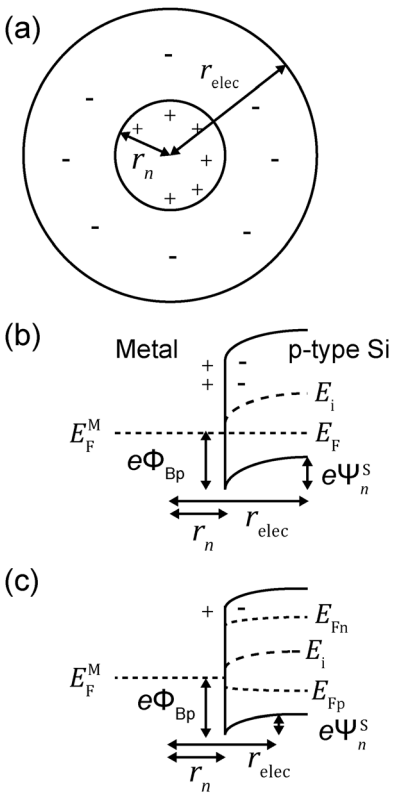

FIG. 1. (a) A charged spherical metal precipitate in the silicon lattice, and the corresponding energy band diagram in (b) thermal equilibrium and (c) under illumination.

The above-described electrostatic effects can be calculated quantitatively with a previously published Schottky junction model of spherical metallic precipitates in Si.[41–44] The model is based on the numerical solution of continuity equations for electrons and holes together with the Poisson equation, enabling the calculation of E_{Fn}, E_{Fp}, and the electrostatic potential, $\Psi_n(r)$, as functions of distance, r, from the precipitate center. Key equations for obtaining the precipitate-limited minority carrier lifetime, τ_{prec}, based on the Schottky model are summarized in the following, and more details are included in the supplementary material.

Recombination activity of metallic precipitates is based upon thermionic emission of charge carriers across the Schottky junction. Thermionic emission current densities of electrons and holes at the precipitate–Si interface can be written as

$$J_e^S = J_e^{sat}\left(\exp\left(\frac{E_{Fn}^S - E_F^M}{k_B T}\right) - 1\right) \tag{3}$$

and

$$J_h^S = -J_h^{sat}\left(\exp\left(\frac{E_F^M - E_{Fp}^S}{k_B T}\right) - 1\right), \tag{4}$$

where J_e^{sat} and J_h^{sat} are the saturation current densities of electrons and holes, respectively, and the superscript S denotes the interface values of the presented quantities. Electrons and holes recombine at the precipitate–Si interface quasi-instantly, which gives the boundary condition at the precipitate surface

$$J_e^S = -J_h^S. \tag{5}$$

The value to which J_e^S converges at a certain generation rate, G, and doping concentration, N_a, can then be used to calculate the recombination rate due to a single precipitate size

$$R_{prec}(n, G, N_a, T) = f_n \times \frac{4\pi r_n^2 \times J_e^S(n, G, N_a, T)}{e}, \tag{6}$$

where f_n is the density of precipitates of size n. Excess electron concentration, Δn_e, is obtained by averaging the r-dependent electron concentration [defined by E_{Fn} and $\Psi_n(r)$] over the simulation domain. Repeating the simulation for several values of G allows the calculation of injection-dependent recombination rate, $R_{prec}(n, \Delta n_e, N_a, T)$. Hence, calculation of the total recombination rate requires knowledge regarding the precipitate size and density distribution in the bulk, that is, the values of f_n at different n. Repeating the calculation for all n allows obtaining the precipitate-limited lifetime, τ_{prec}, through

$$\tau_{prec}(\Delta n_e) = \frac{\Delta n_e}{\sum_n R_{prec}(n, \Delta n_e, N_a, T)}. \tag{7}$$

Here, we note that a useful parametrization exists for calculation of τ_{prec} in cases in which rigorous simulations are unavailable or impractical.[44] Details on calculation of the

precipitate size and density distribution are described in the following sections (III C to III E).

C. Kinetic precipitation model

In this work, Cu precipitation is treated with a kinetic model based on chemical rate equations[40,67]

$$\frac{\partial f_n}{\partial t} = I_{n-1} - I_n, \tag{8}$$

where I_n is the net growth flux of precipitates of size n, f_n is their density as defined above, and $n \geq 2$. Growth and dissolution take place one atom at a time involving two consecutive precipitate sizes and interstitial Cu. Net growth flux of a precipitate from size n to $n+1$ is given by[40]

$$I_n = g_n f_n - d_{n+1} f_{n+1}, \tag{9}$$

where g_n and d_n are, respectively, growth and dissolution rates of n-sized precipitates, and $n \geq 2$.[40] Interstitial Cu atoms are considered precipitates of size 1, and their rate of change is equal to the sum of all net growth fluxes so that[40]

$$\frac{\partial f_1}{\partial t} = -2I_1 - \sum_{n=2}^{\infty} I_n. \tag{10}$$

Integrating the linear system of equations, defined by Eqs. (8)–(10), with respect to time, allows the calculation of full time evolution of precipitate sizes and densities. However, the number of chemical rate equations to solve increases rapidly with precipitate size. To reduce the number of simultaneous calculation events, we use a discretization of f_n according to Ref. 68.

The precipitate growth rate in Eq. (9) can be written as a product of its surface area, A_n, the surface reaction rate constant, k_n, and the interstitial Cu concentration at the precipitate–Si interface, $C_{\mathrm{Cu_i}}(r_n)$[40]

$$g_n = A_n k_n C_{\mathrm{Cu_i}}(r_n). \tag{11}$$

The precipitate dissolution rate, on the other hand, can be written as

$$d_n = A_n k_n C_n^{\mathrm{eq}}, \tag{12}$$

where C_n^{eq} is defined as the interface interstitial Cu concentration at equilibrium with a precipitate of size n, that is, the concentration at which there is no energy change in growth or dissolution ($\Delta G_{n+1} - \Delta G_n = 0$).[40] Therefore, based on Eq. (1), C_n^{eq} in thermal equilibrium can be written as

$$C_n^{\mathrm{eq}} = S_{\mathrm{Cu}}(r_n)\exp\left(\frac{\Delta G_{n+1}^{\mathrm{ex}} - \Delta G_n^{\mathrm{ex}}}{k_{\mathrm{B}}T}\right), \tag{13}$$

where $S_{\mathrm{Cu}}(r_n)$ is the value of solubility at the precipitate–Si interface (discussed further below). The surface reaction rate, k_n, is given by[69]

$$k_n = \frac{D_{\mathrm{Cu}}}{\delta}\exp\left(\frac{\max(\Delta G_{n+1} - \Delta G_n + \Delta G_{\mathrm{act}}, \Delta G_{\mathrm{act}})}{k_{\mathrm{B}}T}\right), \tag{14}$$

where D_{Cu} is the diffusivity of $\mathrm{Cu_i^+}$ affected by ion pairing [calculated according to Eq. (B6) in Reiss *et al.*[66] using intrinsic diffusivity and pairing constant as reported by Istratov *et al.*[48]] δ is the length of a single diffusion step (approximately the lattice spacing of Si), and ΔG_{act} is an activation barrier associated with the chemical reaction of incorporating a Cu atom into the $\mathrm{Cu_3Si}$ precipitate.

D. Solubility of Cu in Si in the dark and under illumination

In this section, solubility of Cu in Si is examined theoretically first of all to evaluate the value of this quantity at the precipitate–Si interface, which is required for the calculation of the dissolution rate in Eq. (12), and second, to consider the effects invoked by carrier injection. As background, there are two mechanisms that increase the solid solubility of Cu in p-type Si in comparison to intrinsic Si. These include first the so-called Fermi level effect,[70] and second, the contribution arising from Cu–B pairing. Taking these mechanisms into account, total Cu solid solubility in thermal equilibrium can be expressed as[71]

$$S_{\mathrm{Cu}} = S_{\mathrm{Cu}}^{\mathrm{int}}\exp\left(\frac{E_{\mathrm{i}} - E_{\mathrm{F}}}{k_{\mathrm{B}}T}\right)(1 + N_{\mathrm{a}}K_{\mathrm{Cu-B}}), \tag{15}$$

where $S_{\mathrm{Cu}}^{\mathrm{int}}$ is the intrinsic solubility from Ref. 72, E_{i} is the intrinsic Fermi level, E_{F} is the Fermi level, and $K_{\mathrm{Cu-B}}$ is the equilibrium constant of Cu–B pairing according to Ref. 48. Very low bulk solubility values of 10^2–10^8 $\mathrm{cm^{-3}}$ for N_{a} of 10^{13}–10^{17} $\mathrm{cm^{-3}}$ are obtained with Eq. (15) at RT (by extrapolating $S_{\mathrm{Cu}}^{\mathrm{int}}$ in Ref. 72). Therefore, at RT, interstitial Cu can be considered supersaturated in all practical cases.

The precipitate–Si interface value of solubility, $S_n(r_n)$ in Eq. (13), is considered in the following. As illustrated in Fig. 1(b), Fermi level pinning causes E_{i} and E_{F} to approach each other at the interface by an amount of energy that corresponds to the band bending. Hence, the magnitude of solubility decreases at the interface by an exponential factor containing the band bending term, and the interface solubility can therefore be written as

$$S_n(r_n) = S_{\mathrm{Cu}}^{\mathrm{int}}\exp\left(\frac{E_{\mathrm{i}}^{\mathrm{bulk}} - e\Psi_n^{\mathrm{S}} - E_{\mathrm{F}}}{k_{\mathrm{B}}T}\right)(1 + N_{\mathrm{a}}K_{\mathrm{Cu-B}}), \tag{16}$$

where $E_{\mathrm{i}}^{\mathrm{bulk}}$ is the bulk value of E_{i} (outside r_{elec}). To avoid any misconceptions related to Eq. (16), although the interface solubility is decreased as compared to the bulk value, it does not mean that the precipitate surface would form a favorable precipitation site as compared to the bulk. As will be shown below in Sec. III E, when viewed from the bulk side (outside r_{elec}), the solubility reduction at the interface is fully compensated by the repulsive force that the electric field of the precipitate directs toward the positively charged $\mathrm{Cu_i^+}$ ions.

Separation of the Fermi level into E_{Fn} and E_{Fp} under illumination poses additional modifications to the expression for the interface solubility. Here, we consider the fact that the solubility of single positively charged interstitial defects

such as Cu_i^+ has been reported to be directly proportional to the concentration of holes.[70] In this case, $S_n(r_n)$ becomes dependent on the quasi-Fermi level of holes at the interface, E_{Fp}^S, such that the interface solubility under carrier injection can be written as

$$S_n(r_n) = S_{Cu}^{int}\exp\left(\frac{E_i^{bulk} - e\Psi_S - E_{Fp}^S}{k_BT}\right)(1 + N_aK_{Cu-B}). \quad (17)$$

Note that in Eq. (17), the effect of illumination is to slightly increase the value of solubility as compared to thermal equilibrium but without major changes at moderate intensities on the order of 1 sun.

E. Electrostatic effects influencing the precipitate growth

In this section, electrostatic effects derived from the built-in electric field around metallic precipitates are considered. Here, we first note that the precipitate growth rate, g_n, defined by Eq. (11), uses the interstitial Cu concentration at the precipitate–Si interface, $C_{Cu_i}(r_n)$, as an input parameter. However, the value of $C_{Cu_i}(r_n)$ depends upon several precipitate size-dependent factors, which complicates the calculation of this quantity. These factors include the electrostatic potential surrounding the precipitate, $\Psi_n(r)$, the interface reaction rate, k_n, the equilibrium interstitial Cu concentration at the precipitate–Si interface, C_n^{eq}, and the precipitate geometry (or radius, r_n, in the spherical case). On the other hand, C_{Cu_i} is independent of the above variables in the bulk, outside of electric fields and concentration gradients associated with the precipitates. In this section, instead of explicitly solving $C_{Cu_i}(r_n)$ for all n as a function of the bulk interstitial Cu concentration denoted in the following as $C_{Cu_i}^{\infty}$, the above mentioned factors are included in new expressions for the growth and dissolution rates, g_n and d_n, that are derived based on the drift-diffusion equation of interstitial Cu.

As charged particles, the movement of Cu_i^+ ions in the Si bulk is governed not only by the diffusion gradient but also by the precipitate-related electric fields. Due to the above noted direct proportionality between [Cu–B] and $[Cu_i^+]$, these effects can be accounted for by writing the drift-diffusion equation directly with respect to the total concentration of interstitial Cu, C_{Cu_i}, as

$$J_{Cu} = e\mu_{Cu}C_{Cu_i}E - eD_{Cu}\nabla C_{Cu_i}, \quad (18)$$

where J_{Cu} is the electric current density carried by Cu_i^+ ions, $\mu_{Cu} = eD_{Cu}/k_BT$ is the mobility of interstitial Cu, and E is the electric field strength. Using Equations (11) and (12) for a spherical precipitate of size n, J_{Cu} can be expressed as a function of distance, r, from the precipitate center

$$J_{Cu}(r) = -\frac{e(g_n - d_{n+1})}{4\pi r^2} = -\frac{4\pi r_n^2 ek_n\left(C_{Cu_i}(r_n) - C_n^{eq}\right)}{4\pi r^2}. \quad (19)$$

Equating (18) and (19), and using $E(r) = -\frac{\partial\Psi_n(r)}{\partial r}$, gives

$$eD_{Cu}\left(\frac{e}{k_BT}\times C_{Cu_i}(r)\times\frac{\partial\Psi_n(r)}{\partial r} + \frac{\partial C_{Cu_i}(r)}{\partial r}\right) = \frac{4\pi r_n^2 ek_n\left(C_{Cu_i}(r_n) - C_n^{eq}\right)}{4\pi r^2}, \quad (20)$$

which can be rearranged to yield

$$eD_{Cu}\exp\left(-\frac{e\Psi_n(r)}{k_BT}\right)\times\frac{\partial}{\partial r}\left(C_{Cu_i}(r)\exp\left(\frac{e\Psi_n(r)}{k_BT}\right)\right) = \frac{4\pi r_n^2 ek_n\left(C_{Cu_i}(r_n) - C_n^{eq}\right)}{4\pi r^2}. \quad (21)$$

Integrating (21) from r_n to r_{elec} will then give

$$C_{Cu_i}(r_{elec})\exp\left(\frac{e\Psi_n(r_{elec})}{k_BT}\right) - C_{Cu_i}(r_n)\exp\left(\frac{e\Psi_n(r_n)}{k_BT}\right) = \beta_n\left(C_{Cu_i}(r_n) - C_n^{eq}\right)\times\int_{r_n}^{r_{elec}} r^{-2}\exp\left(\frac{e\Psi_n(r)}{k_BT}\right)dr, \quad (22)$$

where β_n is defined as

$$\beta_n \equiv \frac{k_nr_n^2}{D_{Cu}}. \quad (23)$$

Defining that the electric potential is zero outside the precipitate-induced electric field $(\Psi(r_{elec}) = 0)$, the precipitate–Si interface value of the potential becomes equal to the built-in voltage (i.e., $\Psi_n(r_n) = \Psi_n^S$). With these definitions, one can solve the interfacial concentration as

$$C_{Cu_i}(r_n) = \frac{1}{1 + \beta_n\mathcal{J}_n}\left(e^{-\frac{e\Psi_n^S}{k_BT}}C_{Cu_i}(r_{elec}) + \beta_n\mathcal{J}_nC_n^{eq}\right), \quad (24)$$

where $\mathcal{J}_n$ is defined as an integral

$$\mathcal{J}_n \equiv \int_{r_n}^{r_{elec}}\frac{\exp\left(\frac{e\left(\Psi_n(r) - \Psi_n^S\right)}{k_BT}\right)}{r^2}dr. \quad (25)$$

Change in precipitate size with respect to time can now be obtained by substituting Eq. (24) into Eq. (19)

$$\frac{\partial n}{\partial t} = g_n - d_{n+1} = -\frac{A_nJ_{Cu}(r_n)}{e} = \frac{4\pi r_n^2k_n\exp\left(-\frac{e\Psi_n^S}{k_BT}\right)}{1 + \beta_n\mathcal{J}_n}\left(C_{Cu_i}(r_{elec}) - C_n^{eq}\exp\left(\frac{e\Psi_n^S}{k_BT}\right)\right). \quad (26)$$

In the following, two notations are defined to simplify the expression in Eq. (26). First, the effective reaction rate, k_{eff}, is defined as

$$k_{eff} \equiv \frac{\exp\left(-\frac{e\Psi_n^S}{k_BT}\right)}{1 + \beta_n\mathcal{J}_n}\times\frac{r_n^2}{r_{elec}^2}\times k_n. \quad (27)$$

Second, effective solubility, S_n^*, is defined as

$$S_n^* \equiv C_n^{eq}\exp\left(\frac{e\Psi_n^S}{k_BT}\right) = S_{Cu}^{int}\exp\left(\frac{E_i^{bulk}-E_{Fp}^S}{k_BT}\right)\exp\left(\frac{\Delta G_{n+1}^{ex}-\Delta G_n^{ex}}{k_BT}\right) \times (1+N_aK_{Cu-B}), \quad (28)$$

where the last equality follows from substituting Eq. (17) into Eq. (28). Using the above notation for k_{eff} and S_n^*, Eq. (26) can be rewritten as

$$g_n - d_{n+1} = A_{elec}k_{eff}\left(C_{Cu_i}(r_{elec}) - S_n^*\right), \quad (29)$$

where $A_{elec} = 4\pi r_{elec}^2$ is the surface area of the volume affected by the electric field [see Fig. 1(a)]. Hence, the effective solubility, S_n^*, can be considered as the equilibrium concentration of interstitial Cu at the outer surface of the volume occupied by the electric field, when the precipitate–Si interface concentration is C_n^{eq}, defined by Eq. (13). Note that, as already mentioned in context with Eq. (16), since the Ψ_n^S term vanishes in Eq. (28), the decrease in the Fermi level effect of solubility at the precipitate–Si interface in Eq. (17) (induced by near-interface bending of E_i) is exactly canceled out in Eq. (28) by the effect of electrostatic repulsion on the equilibrium concentration of interstitial Cu at r_{elec}. Therefore, since only E_{Fp}^S, and not Ψ_n^S, appears in the expression of the effective solubility, S_n^*, illumination plays only a minor role in the energetics of precipitation (meaning that the effective nucleation barrier that includes the electrostatic effects is practically unaffected). Kinetics in Eq. (27), however, is exponentially dependent on the built-in voltage and is therefore expected to depend considerably on the illumination conditions.

Outside of the electric field, the interstitial Cu concentration is defined purely by a spherically symmetric diffusion process toward the volume occupied by the electric field. In analogy to Ref. 40, the growth and dissolution rates can be written with respect to the bulk concentration, $C_{Cu_i}^{\infty}$, and the effective solubility, S_n^*, as

$$g_n = \lambda_{kin}D_{Cu}C_{Cu_i}^{\infty} \quad (30)$$

and

$$d_n = \lambda_{kin}D_{Cu}S_n^*, \quad (31)$$

where λ_{kin} is a kinetic growth factor, defined as

$$\lambda_{kin} \equiv \frac{A_{elec}}{r_{elec} + \frac{D_{Cu}}{k_{eff}}}. \quad (32)$$

Based on the above considerations, determining the correct growth and dissolution rates in the case of charged precipitates with respect to the bulk interstitial Cu concentration, $C_{Cu_i}^{\infty}$, requires the calculation of the surrounding electrostatic potential, $\Psi_n(r)$, with the Schottky model, allowing the calculation of r_{elec} and k_{eff}, and consequently λ_{kin}, which is a direct input parameter in Eqs. (30) and (31). To quantify the effect of illumination on the precipitation kinetics, the dependence of λ_{kin} on the illumination-induced excess carrier concentration is examined in the following section (IV A).

IV. COUPLING OF THE PRECIPITATION MODEL WITH THE SCHOTTKY MODEL

A. Minority carrier concentration dependence of built-in voltage and kinetic growth factor

The built-in voltage, Ψ_n^S, varies considerably depending on the prevailing injection conditions. Ψ_n^S obtained with the Schottky model is plotted on the left axis of Fig. 2 as a function of total electron concentration with model parameters corresponding to small Cu_3Si precipitates in moderately doped Si at RT, that is, $e\Phi_{Bn} = 0.59$ eV (Ref. 73) (where Φ_{Bn} is the Schottky barrier height as measured from the conduction band edge), $[B] = 4.1\times10^{15}\,cm^{-3}$ (≈3.4 Ωcm), $T = 300$ K, and $r_n = 1$ nm. As illustrated, Ψ_n^S is high at the low electron concentration (in the dark, the equilibrium electron concentration is $\approx 2\times10^4\,cm^{-3}$) and quickly decreases when the electron concentration increases through carrier injection. At an electron concentration of $\sim 5\times10^{15}\,cm^{-3}$ (i.e., corresponding to 1 sun illumination in a 400 μm thick polished p-type Si wafer with effective minority carrier lifetime of $\tau_{eff} = 1$ ms), the built-in voltage is slightly negative at $\Psi_n^S \approx -1\times10^{-3}$ V, which means that in this example case the electrostatic barrier for precipitate growth is fully removed under 1 sun. The electrostatic interaction between Cu_i^+ and Cu_3Si precipitates, and consequently the precipitation kinetics, is thus expected to depend to a great extent on the exact illumination/injection conditions.

To illustrate the dependence of precipitation kinetics on injection conditions, the right-side axis of Fig. 2 is plotted with the kinetic growth factor, λ_{kin}, of Eq. (32), which is the only electrostatics-dependent parameter in expressions (30) and (31) defining the growth and dissolution rates. Here, λ_{kin} has been calculated assuming that there is no activation barrier associated with precipitate growth [i.e., $\Delta G_{act} = 0$ in Eq. (14)] and that 1 nm precipitates are larger than the critical

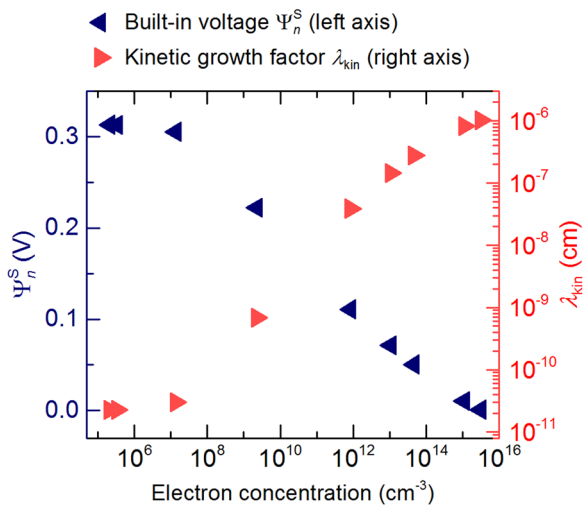

FIG. 2. Electron concentration dependence of the built-in voltage Ψ_n^S (left axis) and the kinetic growth factor λ_{kin} (right axis). Values of $\Phi_{Bn} = 0.59$ V, $[B] = 4.1\times10^{15}\,cm^{-3}$, $T = 300$ K, and $r_n = 1$ nm were used.

size [the slope of the Gibbs energy change in Eq. (1) becomes negative beyond the critical size, i.e., $\Delta G_{n+1} - \Delta G_n < 0$ in Eq. (14)]. With these assumptions, which can be considered realistic based on our results presented in Paper II[76] of this article, one can write the reaction rate of Eq. (14) as $k_n = D_{\mathrm{Cu}}/\delta$, allowing for a solution of λ_{kin} without specifying any of the other unknown energetic parameters in Eq. (2). Based on Fig. 2, the transition from thermal equilibrium (darkness) to electron concentration of $\sim 5 \times 10^{15}\ \mathrm{cm}^{-3}$ (corresponding to 1 sun as described above) increases λ_{kin} over five orders of magnitude. It is therefore highly plausible that illumination can considerably increase the rate at which precipitation progresses in a supersaturated solid solution, and consequently, cause Cu-LID.

B. Modeling Cu-LID lifetime curves

The theory presented in Sec. III allows the calculation of precipitate-limited, injection-dependent minority carrier lifetime, τ_{prec}, during the course of the precipitation process. This section clarifies how this property can be used to simulate Cu-LID minority carrier lifetime curves. The simulations are to be carried out at the wafer level, meaning that, in addition to precipitates, also other recombination mechanisms, including surface and Auger recombination and the BO defect, are considered to be present. A flowchart describing the sequence in which different variables are calculated and their connection within the model is illustrated in Fig. 3.

The simulation begins with the calculation of the excess electron concentration in an illuminated sample, $\Delta n_{\mathrm{e}}^{\mathrm{ill}}$, which can be evaluated iteratively from an equation relating the sample and illumination source-specific generation rate, G, and injection-dependent effective minority carrier lifetime, $\tau_{\mathrm{eff}}(\Delta n_{\mathrm{e}})$

$$\Delta n_{\mathrm{e}}^{\mathrm{ill}} = G \times \tau_{\mathrm{eff}}\left(\Delta n_{\mathrm{e}}^{\mathrm{ill}}\right). \tag{33}$$

The initial $\tau_{\mathrm{eff}}(\Delta n_{\mathrm{e}})$ (at $t = 0$) has to be approximated with an estimation of background, surface, Auger, and radiative recombination-limited lifetime, for example, based on experimental data. After the determination of initial $\Delta n_{\mathrm{e}}^{\mathrm{ill}}$, electrostatic potential distributions, $\Psi_n(r)$, surrounding precipitates of different sizes, corresponding to injection conditions defined by $\Delta n_{\mathrm{e}}^{\mathrm{ill}}$, can be calculated based on the Schottky model. Similarly, the interface quasi-Fermi level of holes in the steady-state, $E_{\mathrm{Fp}}^{\mathrm{S}}$, can be determined. Consequently, using $\Psi_n(r)$ and $E_{\mathrm{Fp}}^{\mathrm{S}}$, key parameters of the precipitation model can be calculated. These include the effective solubility, S_n^*, and the kinetic growth factor, λ_{kin}, which then allow the calculation of the growth and dissolution rates, g_n and d_n, respectively.

Determining g_n and d_n allows for solving the linear system of differential equations for the precipitate size and density distribution defined by Eqs. (8)–(10) over a small time step Δt. After that, injection-dependent τ_{prec} can be determined from the Schottky model, which provides the simulated injection-dependent τ_{eff} after correction for the BO defect, as well as the above-mentioned background, surface, Auger, and radiative recombination-limited lifetime. The BO defect-limited lifetime can be obtained for example from injection-dependent parametrizations of the minority carrier lifetime separately for the slow and the fast recombination stage,[26,45,74] combined with empirical expressions for the recombination activity[26,75] and the degradation rates.[26,46] The injection-dependent τ_{eff} is then used as a basis for calculating $\Delta n_{\mathrm{e}}^{\mathrm{ill}}$ at the next time step from Eq. (33), and τ_{eff} at $\Delta n_{\mathrm{e}} = 0.1 \times N_{\mathrm{a}}$ is used for comparison with experimental data, which means that it is used as one lifetime value in the simulated LID curve.

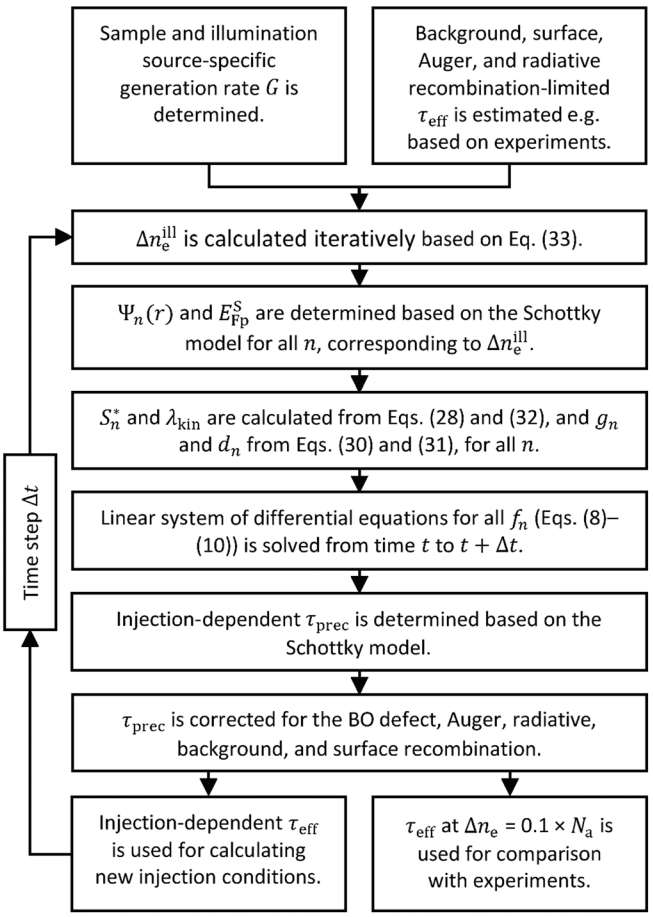

FIG. 3. A flowchart describing the procedure for the simulation of a Cu-LID lifetime curve based on the theory presented in Sec. III.

V. SUMMARY

This article presents a comprehensive model for Cu-related light-induced degradation. Based on previous research in the literature, we have considered highly plausible that Cu-LID is a precipitation process that is kinetically limited in p-type Si by electrostatic repulsion between Cu_3Si precipitates and interstitially diffusing Cu_i^+ ions. A kinetic precipitation model involving spherical metallic precipitates embedded in a semiconducting matrix was constructed based on an earlier model for electrically neutral precipitates. Consequently, precipitate growth and dissolution rates were modified based on the drift-diffusion equation that takes into account changes in precipitate charging and subsequent repulsion of Cu_i^+ ions. In order to determine the necessary electrical parameters at the precipitate–Si interface as a

function of minority carrier injection conditions, the kinetic precipitation model was coupled with a Schottky junction model for metallic precipitates in Si. Based on this approach, it was shown that a transition from thermal equilibrium to illuminated conditions can speed up the precipitation kinetics approximately five orders of magnitude, which is a plausible theoretical explanation for the occurrence of Cu-LID. Since in addition to other electrical parameters, the Schottky junction model enables the calculation of precipitate-limited minority carrier lifetime, one of the main advantages of the proposed model is the possibility to simulate precipitation directly on lifetime level, enabling straightforward comparison with experimental lifetime data. A step-by-step procedure for calculating full Cu-LID curves at the wafer level, when also other recombination mechanisms are present, was demonstrated. In Paper II[76] of this contribution, functionality of the model in reproducing Cu-LID is evaluated through a comparison with experiments.

SUPPLEMENTARY MATERIAL

See supplementary material for a detailed mathematical description of the Schottky junction model for the recombination activity of metallic precipitates.

ACKNOWLEDGMENTS

The work has been funded through the European Research Council under the European Union's FP7 Programme ERC Grant Agreement No. 307315. A.I. acknowledges the financial support of Aalto ELEC doctoral school and Alfred Kordelin Foundation. The authors also acknowledge Professor J. Sinkkonen, whose notes are the base for the derivation in Sec. III E of Paper I, and Dr. Chiara Modanese for valuable comments during manuscript writing.

[1]G. Coletti, Prog. Photovoltaics **21**, 1163 (2013).
[2]D. Macdonald, A. Cuevas, A. Kinomura, Y. Nakano, and L. J. Geerligs, J. Appl. Phys. **97**, 033523 (2005).
[3]A. A. Istratov and E. R. Weber, J. Electrochem. Soc. **149**, G21 (2002).
[4]S. Choi, B. Jang, J. Kim, H. Song, and M. Han, Sol. Energy **125**, 198 (2016).
[5]K. Graff, *Metal Impurities in Silicon-Device Fabrication* (Springer-Verlag, Berlin, 1999).
[6]J. Bartsch, A. Mondon, K. Bayer, C. Schetter, M. Hörteis, and S. W. Glunz, J. Electrochem. Soc. **157**, H942 (2010).
[7]A. ur Rehman and S. H. Lee, Materials **7**, 1318 (2014).
[8]S. Flynn and A. Lennon, Sol. Energy Mater. Sol. Cells **130**, 309 (2014).
[9]A. Kraft, C. Wolf, J. Bartsch, and M. Glatthaar, Energy Procedia **67**, 93 (2015).
[10]A. Kraft, C. Wolf, J. Bartsch, M. Glatthaar, and S. Glunz, Sol. Energy Mater. Sol. Cells **136**, 25 (2015).
[11]W. B. Henley, D. A. Ramappa, and L. Jastrezbski, Appl. Phys. Lett. **74**, 278 (1999).
[12]R. Sachdeva, A. A. Istratov, and E. R. Weber, Appl. Phys. Lett. **79**, 2937 (2001).
[13]I. Tarasov and O. Ostapenko, in *Eighth Workshop on Crystalline Silicon Solar Cell Materials and Processes, Copper Mountain, Colorado, USA, 17–19 August 1998*, edited by R. Sinton, T. Tan, J. Kalejs, J. Gee, M. Stavola, T. Saitoh, R. Swanson, and B. Sopori. (NREL, Golden, CO, USA, 1998), pp. 207–210.
[14]D. A. Ramappa, Appl. Phys. Lett. **76**, 3756 (2000).
[15]M. Yli-Koski, M. Palokangas, A. Haarahiltunen, H. Väinölä, J. Storgårds, H. Holmberg, and J. Sinkkonen, J. Phys.: Condens. Matter **14**, 13119 (2002).
[16]H. Väinölä, M. Yli-Koski, A. Haarahiltunen, and J. Sinkkonen, J. Electrochem. Soc. **150**, G790 (2003).
[17]M. Yli-Koski, H. Väinölä, A. Haarahiltunen, J. Storgårds, E. Saarnilehto, and J. Sinkkonen, Phys. Scr. **T114**, 69 (2004).
[18]A. Belayachi, T. Heiser, J. P. Schunck, and A. Kempf, Appl. Phys. A **80**, 201 (2005).
[19]H. Väinölä, E. Saarnilehto, M. Yli-Koski, A. Haarahiltunen, J. Sinkkonen, G. Berenyi, and T. Pavelka, Appl. Phys. Lett. **87**, 032109 (2005).
[20]H. Savin, M. Yli-Koski, and A. Haarahiltunen, Appl. Phys. Lett. **95**, 152111 (2009).
[21]J. Lindroos and H. Savin, Sol. Energy Mater. Sol. Cells **147**, 115 (2016).
[22]J. Lindroos, Y. Boulfrad, M. Yli-Koski, and H. Savin, J. Appl. Phys. **115**, 154902 (2014).
[23]T. Turmagambetov, S. Dubois, J. P. Garandet, B. Martel, N. Enjalbert, J. Veirman, and E. Pihan, Phys. Status Solidi C **11**, 1697 (2014).
[24]J. Schmidt, A. G. Aberle, and R. Hezel, in Conference Record of the Twenty Sixth IEEE Photovoltaic Specialists Conference - 1997, *Anaheim, California, USA, 29 September–3 October 1997*, edited by Anonymous (IEEE, New York, 1997), pp. 13–18.
[25]J. Schmidt and K. Bothe, Phys. Rev. B **69**, 24107-1 (2004).
[26]V. V. Voronkov, R. Falster, K. Bothe, B. Lim, and J. Schmidt, J. Appl. Phys. **110**, 063515 (2011).
[27]T. Dullweber and J. Schmidt, IEEE J. Photovoltaics **6**, 1366 (2016).
[28]K. Ramspeck, S. Zimmermann, H. Nagel, A. Metz, Y. Gassenbauer, B. Birkmann, and A. Seidl, in *Proceedings of the 27th European Photovoltaic Solar Energy Conference, Frankfurt, Germany, 24–28 September 2012*, edited by S. Nowak, A. Jäger-Waldau, and P. Helm. (WIP, Munich, Germany, 2012), pp. 861–865.
[29]F. Fertig, K. Krauß, and S. Rein, Phys. Status Solidi RRL **9**, 41 (2015).
[30]F. Kersten, P. Engelhart, H. C. Ploigt, A. Stekolnikov, T. Lindner, F. Stenzel, M. Bartzsch, A. Szpeth, K. Petter, J. Heitmann, and J. W. Müller, Sol. Energy Mater. Sol. Cells **142**, 83 (2015).
[31]K. Krauss, F. Fertig, D. Menzel, and S. Rein, Energy Procedia **77**, 599 (2015).
[32]F. Kersten, P. Engelhart, H. C. Ploigt, F. Stenzel, K. Petter, T. Lindner, A. Szpeth, M. Bartzsch, A. Stekolnikov, and M. Scherff, in *Proceedings of the 31st European Photovoltaic Solar Energy Conference, Hamburg, Germany, 14–18 September 2015*, edited by S. Rinck (WIP, Munich, Germany, 2015), pp. 1830–1834.
[33]K. Y. Yen, S. P. Su, S. H. T. Chen, and L. W. Cheng, in *2015 IEEE 42nd Photovoltaic Specialist Conference (PVSC), New Orleans, 14–19 June 2015*, edited by Anonymous (IEEE, New York, 2015), pp. 1–3.
[34]D. N. R. Payne, C. E. Chan, B. J. Hallam, B. Hoex, M. D. Abbott, S. R. Wenham, and D. M. Bagnall, Phys. Status Solidi RRL **10**, 237 (2016).
[35]D. Bredemeier, D. Walter, S. Herlufsen, and J. Schmidt, AIP Adv. **6**, 035119 (2016).
[36]K. Nakayashiki, J. Hofstetter, A. E. Morishige, T. A. Li, D. B. Needleman, M. A. Jensen, and T. Buonassisi, IEEE J. Photovoltaics **6**, 860 (2016).
[37]A. E. Morishige, M. A. Jensen, D. B. Needleman, K. Nakayashiki, J. Hofstetter, T. T. A. Li, and T. Buonassisi, IEEE J. Photovoltaics **6**, 1466 (2016).
[38]C. E. Chan, D. N. R. Payne, B. J. Hallam, M. D. Abbott, T. H. Fung, A. M. Wenham, B. S. Tjahjono, and S. R. Wenham, IEEE J. Photovoltaics **6**, 1473 (2016).
[39]D. Kashchiev, *Nucleation* (Butterworth-Heinemann, Oxford, 2000), pp. 115–135.
[40]S. T. Dunham, J. Electrochem. Soc. **142**, 2823 (1995).
[41]P. S. Plekhanov and T. Y. Tan, Appl. Phys. Lett. **76**, 3777 (2000).
[42]M. D. Negoita and T. Y. Tan, J. Appl. Phys. **94**, 5064 (2003).
[43]W. Kwapil, J. Schön, F. Schindler, W. Warta, and M. C. Schubert, IEEE J. Photovoltaics **4**, 791 (2014).
[44]W. Kwapil, J. Schön, W. Warta, and M. C. Schubert, IEEE J. Photovoltaics **5**, 1285 (2015).
[45]T. Niewelt, J. Schön, J. Broisch, W. Warta, and M. Schubert, Phys. Status Solidi RRL **9**, 692 (2015).
[46]J. Schön, T. Niewelt, J. Broisch, W. Warta, and M. C. Schubert, J. Appl. Phys. **118**, 245702 (2015).
[47]R. N. Hall and J. H. Racette, J. Appl. Phys. **35**, 379 (1964).
[48]A. A. Istratov, C. Flink, H. Hieslmair, E. R. Weber, and T. Heiser, Phys. Rev. Lett. **81**, 1243 (1998).
[49]A. A. Istratov, H. Hieslmair, C. Flink, T. Heiser, and E. R. Weber, Appl. Phys. Lett. **71**, 2349 (1997).
[50]A. A. Istratov, C. Flink, H. Hieslmair, T. Heiser, and E. R. Weber, Appl. Phys. Lett. **71**, 2121 (1997).

[51]T. Heiser, S. McHugo, H. Hieslmair, and E. R. Weber, Appl. Phys. Lett. **70**, 3576 (1997).
[52]M. B. Shabani, T. Yoshimi, and H. Abe, J. Electrochem. Soc. **143**, 2025 (1996).
[53]J. Lindroos and H. Savin, J. Appl. Phys. **116**, 234901 (2014).
[54]A. A. Istratov, H. Hedemann, M. Seibt, O. F. Vyvenko, W. Schröter, T. Heiser, C. Flink, H. Hieslmair, and E. R. Weber, J. Electrochem. Soc. **145**, 3889 (1998).
[55]C. Flink, H. Feick, S. A. McHugo, W. Seifert, H. Hieslmair, T. Heiser, A. A. Istratov, and E. R. Weber, Phys. Rev. Lett. **85**, 4900 (2000).
[56]M. L. W. Thewalt, M. Steger, A. Yang, N. Stavrias, M. Cardona, H. Riemann, N. V. Abrosimov, M. F. Churbanov, A. V. Gusev, A. D. Bulanov, I. D. Kovalev, A. K. Kaliteevskii, O. N. Godisov, P. Becker, H. J. Pohl, J. W. Ager III, and E. E. Haller, Physica B **401–402**, 587 (2007).
[57]A. Inglese, J. Lindroos, H. Vahlman, and H. Savin, J. Appl. Phys. **120**, 125703 (2016).
[58]M. Boehringer, J. Hauber, S. Passefort, and K. Eason, J. Electrochem. Soc. **152**, G1 (2005).
[59]H. W. Guo and S. T. Dunham, Appl. Phys. Lett. **89**, 182106 (2006).
[60]A. A. Istratov and E. R. Weber, Appl. Phys. A **66**, 123 (1998).
[61]J. W. Christian, *The Classical Theory of Nucleation* (Pergamon Press, Oxford, 2002).
[62]D. Porter, K. Easterling, and M. Sherif, *Phase Transformations in Metals and Alloys* (CRC Press, Boca Raton, 2009).
[63]F. R. N. Nabarro, Proc. Phys. Soc. **52**, 90 (1940).
[64]M. Seibt, M. Griess, A. A. Istratov, H. Hedemann, A. Sattler, and W. Schröter, Phys. Status Solidi A **166**, 171 (1998).
[65]M. Seibt, H. Hedemann, A. A. Istratov, F. Riedel, A. Sattler, and W. Schröter, Phys. Status Solidi A **171**, 301 (1999).
[66]H. Reiss, C. S. Fuller, and F. J. Morin, Bell Syst. Tech. J. **35**, 535 (1956).
[67]A. Haarahiltunen, H. Väinölä, O. Anttila, E. Saarnilehto, M. Yli-Koski, J. Storgårds, and J. Sinkkonen, Appl. Phys. Lett. **87**, 151908 (2005).
[68]S. Kobayashi, J. Cryst. Growth **174**, 163 (1997).
[69]M. Schrems, *Oxygen in Silicon* (Academic Press Limited, London, 1994), pp. 391–447.
[70]W. Shockley and J. L. Moll, Phys. Rev. **119**, 1480 (1960).
[71]R. Hoelzl, K. J. Range, and L. Fabry, Appl. Phys. A **75**, 525 (2002).
[72]E. R. Weber, Appl. Phys. A **30**, 1 (1983).
[73]M. O. Aboelfotoh, A. Cros, B. G. Svensson, and K. N. Tu, Phys. Rev. B **41**, 9819 (1990).
[74]J. D. Murphy, K. Bothe, R. Krain, V. V. Voronkov, and R. J. Falster, J. Appl. Phys. **111**, 113709 (2012).
[75]K. Bothe, R. Sinton, and J. Schmidt, Prog. Photovoltaics **13**, 287 (2005).
[76]H. Vahlman, A. Haarahiltunen, W. Kwapil, J. Schön, A. Inglese, and H. Savin, "Modeling of light-induced degradation due to Cu precipitation in p-type silicon. II. Comparison of simulations and experiments," J. Appl. Phys. **121**, 195704 (2017).